Time sequence and time scale of intermediate mass fragment emission

E. De Filippo,[1] A. Pagano,[1] J. Wilczyński,[2,*] F. Amorini,[3] A. Anzalone,[3] L. Auditore,[4] V. Baran,[3] I. Berceanu,[5] J. Blicharska,[6] J. Brzychczyk,[7] A. Bonasera,[3] B. Borderie,[8] R. Bougault,[9] M. Bruno,[10] G. Cardella,[1] S. Cavallaro,[3] M. B. Chatterjee,[11] A. Chbihi,[12] J. Cibor,[13] M. Colonna,[3] M. D'Agostino,[10] R. Dayras,[14] M. Di Toro,[3] J. Frankland,[12] E. Galichet,[8] W. Gawlikowicz,[7] E. Geraci,[10] F. Giustolisi,[3] A. Grzeszczuk,[6] P. Guazzoni,[15] D. Guinet,[16] M. Iacono-Manno,[3] S. Kowalski,[6] E. La Guidara,[3] G. Lanzanò,[1] G. Lanzalone,[3] N. Le Neindre,[8] S. Li,[17] C. Maiolino,[3] Z. Majka,[7] M. Papa,[1] M. Petrovici,[5] E. Piasecki,[18] S. Pirrone,[1] R. Płaneta,[7] G. Politi,[1] A. Pop,[5] F. Porto,[3] M. F. Rivet,[8] E. Rosato,[19] F. Rizzo,[3] S. Russo,[15] P. Russotto,[3] M. Sassi,[15] K. Schmidt,[6] K. Siwek-Wilczyńska,[18] I. Skwira,[18] M. L. Sperduto,[3] Ł. Świderski,[18] A. Trifirò,[4] M. Trimarchi,[4] G. Vannini,[10] M. Vigilante,[19] J. P. Wieleczko,[12] H. Wu,[17] Z. Xiao,[17] L. Zetta,[15] and W. Zipper[6]

[1]*INFN, Sezione di Catania and Dipartimento di Fisica e Astronomia, Università di Catania, Italy*
[2]*A. Sołtan Institute for Nuclear Studies, Swierk/Warsaw, Poland*
[3]*INFN, Laboratori Nazionali del Sud and Dipartimento di Fisica e Astronomia, Università di Catania, Italy*
[4]*INFN, Gruppo Collegato di Messina and Dipartimento di Fisica, Università di Messina, Italy*
[5]*Institute for Physics and Nuclear Engineering, Bucharest, Romania*
[6]*Institute of Physics, University of Silesia, Katowice, Poland*
[7]*M. Smoluchowski Institute of Physics, Jagellonian University, Cracow, Poland*
[8]*Institut de Physique Nucléaire, IN2P3-CNRS, Orsay, France*
[9]*LPC, ENSI Caen and Université de Caen, France*
[10]*INFN, Sezione di Bologna and Dipartimento di Fisica, Università di Bologna, Italy*
[11]*Saha Institute of Nuclear Physics, Kolkata, India*
[12]*GANIL, CEA, IN2P3-CNRS, Caen, France*
[13]*H. Niewodniczański Institute of Nuclear Physics, Cracow, Poland*
[14]*DAPNIA/SPhN, CEA-Saclay, France*
[15]*INFN, Sezione di Milano and Dipartimento di Fisica, Università di Milano, Italy*
[16]*IPN, IN2P3-CNRS and Université Claude Bernard, Lyon, France*
[17]*Institute of Modern Physics, Lanzhou, China*
[18]*Institute of Experimental Physics, Warsaw University, Warsaw, Poland*
[19]*INFN, Sezione Napoli and Dipartimento di Fisica, Università di Napoli, Italy*

(Received 2 December 2004; published 14 April 2005)

Semiperipheral collisions in the ^{124}Sn+^{64}Ni reaction at 35 MeV/nucleon were studied using the forward part of the Charged Heavy Ion Mass and Energy Resolving Array. Nearly completely determined ternary events involving projectilelike fragments (PLF), targetlike fragments (TLF), and intermediate mass fragments (IMF) were selected. A new method of studying the reaction mechanism, focusing on the analysis of the correlations between relative velocities in the IMF+PLF and IMF+TLF subsystems, is proposed. The relative velocity correlations provide information on the time sequence and time scale of the neck fragmentation processes leading to production of IMFs. It is shown that the majority of light IMFs are produced within 40–80 fm/c after the system starts to reseparate. Heavy IMFs are formed at times of about 120 fm/c or later and can be viewed as resulting from two-step (sequential) neck rupture processes.

DOI: 10.1103/PhysRevC.71.044602 PACS number(s): 25.70.Mn, 25.70.Pq

I. INTRODUCTION

In nucleus-nucleus collisions at intermediate energies (20–100 MeV/nucleon) one can observe phenomena characteristic of the transition from the dynamics driven by the mean field to the dynamics dominated by short mean-free path nucleon-nucleon interactions. Special attention is often paid to semiperipheral collisions because this is the best way to study well-localized processes taking place in the zone of contact between two colliding nuclei. The interaction zone undergoes the most interesting dynamical evolution: in the early stage of the reaction it absorbs most of the heat generated by nucleon-nucleon collisions, and later, during the process of reseparation, it may evolve into a transient necklike structure between both nuclei. The interaction zone is thus a precursor of the participant midrapidity source, easily identified at relativistic energies, and the necklike structure can be viewed as a low-energy analog of the participant zone during its expansion stage.

Experimental studies of nucleus-nucleus collisions at intermediate energies have revealed that at least at lower energies of 20–40 MeV/nucleon, semiperipheral reactions are basically binary. The observed projectilelike fragments (PLF) and targetlike fragments (TLF) are products of deexcitation (via evaporation of neutrons and light charged particles) of primary products of binary reactions (see recent review article of Schröder and Tōke [1] and references therein).

*Electronic address: wilczynski@ipj.gov.pl

However, along with PLFs, TLFs and evaporated light charged particles, a new class of reaction products, intermediate mass fragments (IMF) gradually become visible [2–7]. Usually, all fragments of $Z \geqslant 3$ are classified as IMFs. Light fragments dominate among IMFs, but their mass spectrum extends (nearly exponentially) to quite heavy fragments (see, e.g., Ref. [6]). In the case of massive IMFs there is a problem of distinguishing them from PLFs and/or TLFs by relying only on the charge.

The IMF production intensifies with increasing bombarding energy and centrality of the collision. Expansion of the participant zone in nearly central collisions leads to abundant production of IMFs. Their energy spectra and production cross sections provide valuable information on the nuclear equation of state and dynamical properties of hot nuclear matter (see review articles of Borderie [8] and Chomaz, Colonna, and Randrup [9] and references therein).

In the present article we concentrate our study on semiperipheral reactions in which one can observe production of IMFs in easy-to-analyze final-state configurations involving only one IMF accompanying the PLF and TLF. We show that IMFs are predominantly emitted from the dynamically expanding neck region, either almost promptly (when both main fragments are still in close proximity) or sequentially, that is, from the projectile or target fragment some time after the reseparation of the binary system but early enough to maintain memory of the neck configuration manifested by nearly collinear motion of all three fragments. We demonstrate that from the analysis of relative energies in both IMF+PLF and IMF+TLF subsystems (for a class of almost completely determined ternary events involving the PLF, TLF, and one IMF) we can infer the times of formation of the IMFs within first 120–150 fm/c after the reseparation. Longer times, exceeding 150 fm/c, cannot be differentiated with the proposed method and then only the lower limit for the emission time can be established.

The aligned ternary reactions observed in our experiment are consistent with predictions of the dynamic model based on microscopic transport equations of Boltzmann-Nordheim-Vlasov (BNV) [10]. The mechanism of nearly prompt emission of relatively light IMFs from the neck region observed both, in experiment and in model simulations, can be viewed as the precursor of the fragmentation mechanism in the participant zone—developing to full-scale multifragmentation at smaller impact parameters and higher energies. Conversely, emission of heavier IMFs is shown to happen at the late stage of the neck expansion process and can be associated with the scenario of "dynamical fission" reactions [5,11–13].

II. EXPERIMENT

The advantage of focusing the reaction products at forward angles combined with reliable detection and recognition of PLFs, TLFs, and IMFs as unambiguous as possible dictated the choice of a reaction in the *inverse* kinematics. The TLFs are then fast enough in the laboratory system for their detection and precise energy measurements, whereas the velocities of the three groups of fragments mentioned above are sufficiently differentiated. For these reasons, the ^{124}Sn+^{64}Ni reaction at projectiles' energy, $E(^{124}\mathrm{Sn}) = 35$ MeV/nucleon, was chosen for the present experiment. Nucleus-nucleus collisions in this system were studied as part of the REVERSE Collaboration program [14,15]. The experiment was carried out at the Laboratorio Nazionale del Sud in Catania. The ^{124}Sn beam was accelerated to an energy of 35 MeV/nucleon in the LNS Super-Conducting Cyclotron. The beam bombarded a ^{64}Ni target (310 μg/cm^2 thick), placed inside the Charged Heavy Ion Mass and Energy Resolving Array (CHIMERA) designed [16] for studying nucleus-nucleus collisions in 4π geometry. Only the forward part of the multidetector system, consisting of 688 detection cells arranged in nine rings covering the angular range from 1° to 30°, with full 2π azimuthal symmetry around the beam axis, was used in this inverse kinematics experiment. A single detection cell of the CHIMERA multidetector consists of a planar 300-μm silicon detector (200 μm for the most forward angles) followed by a CsI(Tl) scintillator with a thickness ranging from 3 cm at backward angles to 12 cm at the most forward angles. Three identification techniques are simultaneously used in CHIMERA.

First, the $\Delta E - E$ technique is employed for Z identification of fragments punching through the silicon detectors and additionally for *isotopic* identification of IMFs with atomic numbers $Z < 10$.

Second, mass identification is performed via the time-of-flight (TOF) measurement using the timing signal from silicon detectors with respect to the timing of the high-frequency signal from the cyclotron. An overall time resolution of $\delta t \approx 0.8$ ns (FWHM) was achieved. The TOF technique is basically used for velocity measurements for heavy ions of $Z > 2$ detected in the forward part of CHIMERA with flight paths in the range from 1 to 3 m. This technique is essential for mass and (indirectly) charge determination of slow TLFs stopped in front silicon detectors.

Third, energetic light charged particles, stopped in the scintillator crystal, are identified by applying the pulse-shape discrimination (PSD) method. More details concerning design, capabilities, and detection techniques used in the CHIMERA multidetector can be found in Refs. [16–18].

III. ANALYSIS OF EXPERIMENTAL DATA

Experimental data on ^{124}Sn+^{64}Ni collisions at 35 MeV/nucleon have been collected with the beam intensity of about 5×10^7 particles/s, sufficiently low to minimize pileup events. In total, 3×10^7 events triggered by the condition of a charged particle multiplicity $M \geqslant 3$ were recorded (in a part of the experiment $M \geqslant 2$ events were also accepted). Events best representing a class of central collisions have been separately analyzed in Ref. [19]. This work concentrates on those semiperipheral collisions that can be almost completely reconstructed thanks to nearly 100% detection efficiency for charged particles emitted within the angular range of the CHIMERA detector. Our special interest has been focused on almost completely reconstructed "nearly ternary" reactions, in which, apart from remnants of the projectile and target nuclei, PLF and TLF, respectively (and some light particles

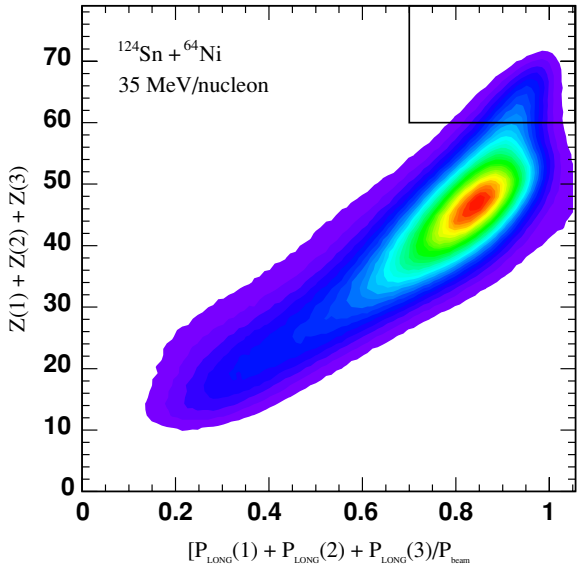

FIG. 1. (Color online) Sum of the charges of three heaviest fragments, $Z(1) + Z(2) + Z(3)$, as a function of their combined longitudinal momentum (divided by the beam particle momentum), $[P_{\rm long}(1) + P_{\rm long}(2) + P_{\rm long}(3)]/P_{\rm beam}$, in the ^{124}Sn+^{64}Ni reaction at an energy of ^{124}Sn projectiles of 35 MeV/nucleon. Limits given by Eqs. (1) and (2) are shown in the upper right corner.

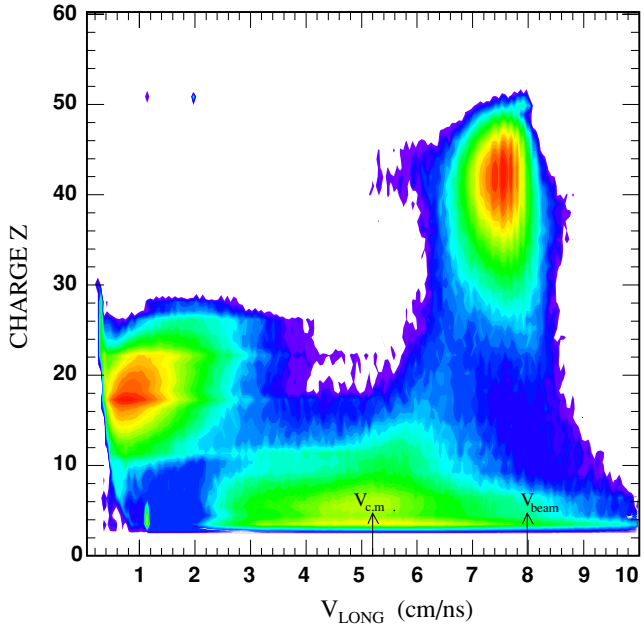

FIG. 2. (Color online) Fragments' distribution in "nearly ternary" events satisfying conditions of Eqs. (1) and (2). Atomic numbers $Z(i)$ of three heaviest fragments in a given event are displayed as a function of their longitudinal velocities $V_{\rm long}(i)$. Localization of the fragments in three different, well-separated regions is used as criterion for identifying these fragments as PLF, TLF, and IMF.

of $Z \leqslant 2$), also a third fragment, an IMF of $Z \geqslant 3$ was detected.

A. Selection of ternary events

To select the class of almost completely reconstructed three-fragment events, we present in Fig. 1 the sum of the charge of the three heaviest fragments, $Z(1) + Z(2) + Z(3)$, versus the sum of their longitudinal momenta divided by the beam particle momentum, $[P_{\rm long}(1) + P_{\rm long}(2) + P_{\rm long}(3)]/P_{\rm beam}$. The upper right-hand-side end of this distribution represents "nearly ternary" events, in which a small missing charge and momentum can be attributed to preequilibrium emission and/or evaporation of light particles of $Z \leqslant 2$ at various stages of the reaction. For further analysis we have selected events satisfying the condition:

$$Z(1) + Z(2) + Z(3) > 60. \qquad (1)$$

As it is seen from Fig. 1, the above condition automatically implies that these three heaviest fragments jointly carry the longitudinal momentum equal to at least 70% of the projectile momentum:

$$P_{\rm long}(1) + P_{\rm long}(2) + P_{\rm long}(3) > 0.7\, P_{\rm beam}. \qquad (2)$$

We have checked that in this subset of events the fourth detected fragment (if any) was *always* a hydrogen or at most helium isotope, $Z(4) \leqslant 2$. Therefore probability that another (undetected) IMF was produced in this selected subset of events was rather low. Our selected set of events (about 3×10^5 events in total) represents only a small portion (about 1%) of the total number of the events recorded in the experiment under the condition $M \geqslant 3$.

In the following, we analyze the selected set of nearly ternary events with the aim of studying the mechanism of reactions with three fragments in the final state—naturally representing the transition from binary reactions (or fusion), most probable at low energies, to more complex multibody reactions that dominate at intermediate energies.

As mentioned previously, conditions of the inverse kinematics of the studied ^{124}Sn+^{64}Ni reaction greatly facilitate the detection and easy distinction of PLFs, TLFs, and IMFs. For separation of these three species of reaction products we use both, charge- and longitudinal velocity distributions. Figure 2 shows the two-dimensional distribution of three heaviest fragments as a function of Z of a given fragment and its longitudinal velocity $V_{\rm long}$, for all nearly ternary events selected with conditions (1) and (2). Thus each ternary event is represented in Fig. 2 with three points. One can easily see three groups of fragments that can be unmistakably separated and recognized as PLFs, TLFs, and IMFs. The projectilelike fragments, PLF, cover the area corresponding to heavy and relatively fast fragments of Z values approaching the Z of the Sn projectile, $Z_{\rm proj} = 50$, and moving with velocities of about 7.5 cm/ns, that is, somewhat slower than projectiles ($V_{\rm proj} = 8.0$ cm/ns). Targetlike fragments, TLF, are grouped in the region around $Z \approx 18$ and $V_{\rm par} \approx 1$ cm/ns. The entire region of intermediate velocities encloses third species of reaction products, intermediate mass fragments, IMF. It is seen from Fig. 2 that IMFs are mostly light fragments, but this group

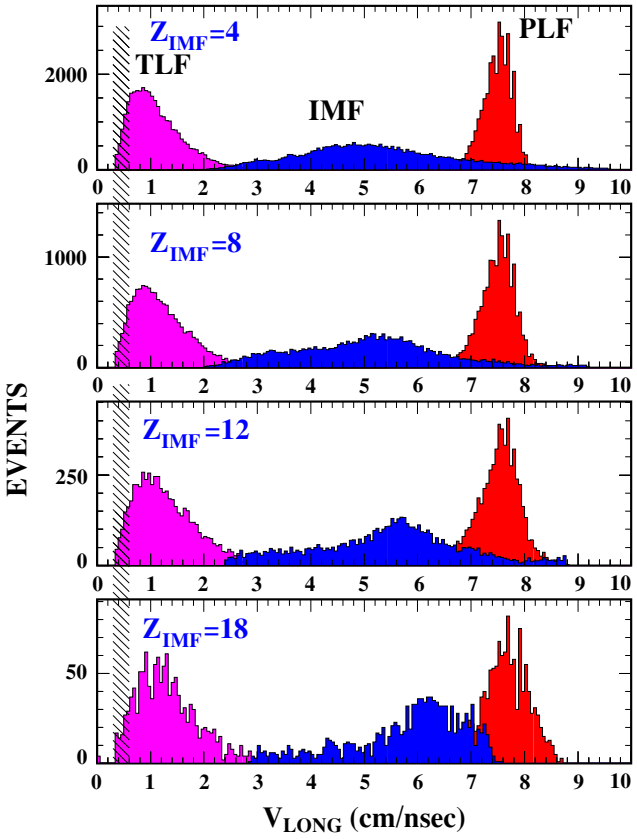

FIG. 3. (Color online) Longitudinal velocity distributions of PLFs, TLFs, and IMFs for selected IMF charges, $Z_{\rm IMF} = 4$, 8, 12, and 18, obtained by using two-dimensional contours in the Z vs. $V_{\rm long}$ plane (see Fig. 2) as gates to define the PLF, TLF, and IMF. The dashed area indicates detection thresholds.

of reaction products extends also toward larger Z values, up to $Z \approx 25$.

B. Velocity distributions of PLFs, TLFs, and IMFs

For further analysis, the well-distinguished three groups of fragments (PLFs, TLFs, and IMFs) were separated by applying contour gates in the Z vs. $V_{\rm long}$ distribution. As shown in Fig. 2, the recognition of PLFs, TLFs, and IMFs on the grounds of their localization in the Z vs. $V_{\rm long}$ plane is well justified. In Fig. 3 we show the longitudinal velocity spectra of PLFs, TLFs, and IMFs gated by respective two-dimensional contours in the Z vs. $V_{\rm long}$ plane. The projections are done separately for selected values of $Z_{\rm IMF} = 4$, 8, 12, and 18.

A clear distinction between PLFs, TLFs, and IMFs, seen in Fig. 2, is maintained in two-dimensional distributions of the selected nearly ternary events plotted as a function of the longitudinal and transverse velocities. The $V_{\rm trans}$ vs. $V_{\rm long}$ plots are shown in Figs. 4 and 5, separately for selected light IMFs ($Z_{\rm IMF} = 4$) and heavy IMFs ($Z_{\rm IMF} = 12$). Similarly as in Fig. 2, each ternary event is represented by three points showing positions of PLF, TLF, and IMF. Fragments recognized according to their localization in Z vs. $V_{\rm long}$ diagram as

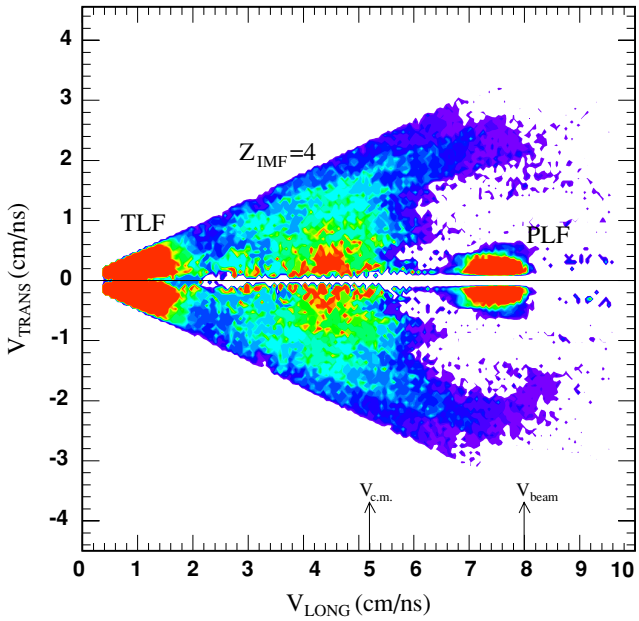

FIG. 4. (Color online) Distribution of "ternary" events satisfying conditions of Eqs. (1) and (2), selected for a fixed charge of the intermediate mass fragment $Z_{\rm IMF} = 4$. Transverse vs. longitudinal velocities of all three fragments detected in a given event (PLF, TLF, and IMF) are displayed jointly. Angular range of the forward part of the CHIMERA multidetector ($\theta \leqslant 30^\circ$) limits the detected events.

IMFs (see Fig. 2) can be quite distinctively separated from PLFs and TLFs also in $V_{\rm trans}$ vs. $V_{\rm long}$ distributions. Figures 4 and 5, as well as the projected spectra shown in Fig. 3, demonstrate the essential features of the IMFs distributions: First of all, IMFs are emitted with longitudinal velocities that are usually intermediate between those of PLF and TLF. Closer

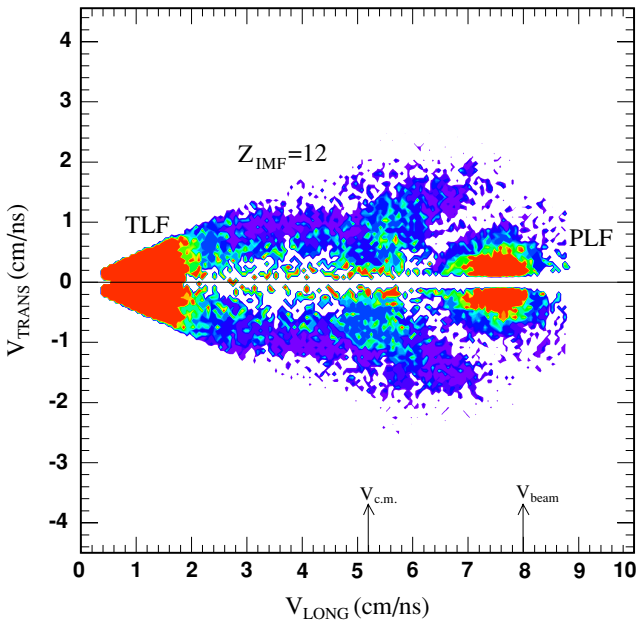

FIG. 5. (Color online) Same as Fig. 3, except for $Z_{\rm IMF} = 12$.

examination of the velocity distributions shows that the average longitudinal velocity of IMFs cannot be identified with the velocity of the center-of-mass (indicated in Figs. 4 and 5 by arrows) or with half of the beam velocity, $V_{\rm beam}/2$, representing the velocity of the reference frame for nucleon-nucleon collisions. The velocity spectra displayed in Fig. 3 show that the average longitudinal velocity of light IMFs ($Z_{\rm IMF} = 4$) can be rather correlated with the midvelocity, halfway between the longitudinal velocities of the TLF and PLF:

$$V_{\rm mid} = \tfrac{1}{2}\left[\left\langle V_{\rm long}^{\rm PLF}\right\rangle + \left\langle V_{\rm long}^{\rm TLF}\right\rangle\right]. \qquad (3)$$

For heavier fragments the observed velocities are even somewhat larger (see the lower panel in Fig. 3). All these observations are consistent with the rather generally accepted hypothesis that IMFs are emitted from the neck zone connecting PLF and TLF during reseparation of these two fragments.

It is very instructive to compare diagrams of Fig. 4 and 5 with results of the theoretical simulation of the studied semiperipheral collisions in the ^{124}Sn+^{64}Ni system, carried out in terms of the stochastic dynamical model based on Boltzmann-Nordheim-Vlasov (BNV) transport equations [10]. In Fig. 6 we show the simulated theoretical events plotted in the same way as experimental events in Figs. 4 and 5. Only ternary events were selected for this projection. Because of low statistics of very time-consuming theoretical simulations, Fig. 6 combines results for all IMFs, undifferentiated according to their mass or charge. The displayed events were generated assuming semiperipheral collisions at impact parameters ranging from $b = 5$ fm to $b = 8$ fm [10]. It is seen that the essential features of the experimental $V_{\rm trans}$ vs. $V_{\rm long}$ distributions: characteristic localization of PLFs, TLFs, and IMFs, as well as the average values of $V_{\rm long}$ for these three groups of fragments are well reproduced in the theoretical simulation. (The theoretical distribution of fragments in Fig. 6 should be compared in the first place with the data for $Z_{\rm IMF} = 4$, shown in Fig. 4, because the majority of IMFs are light fragments.)

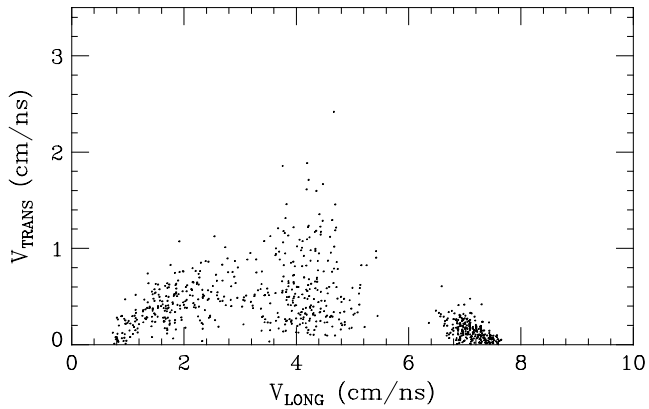

FIG. 6. Transverse vs. longitudinal velocity distribution of ternary events in semiperipheral ^{124}Sn+^{64}Ni collisions at 35 MeV/nucleon simulated in the stochastic Boltzmann-Nordheim-Vlasov transport model [10]. The displayed events were generated assuming collisions at impact parameters ranging from $b = 5$ fm to $b = 8$ fm.

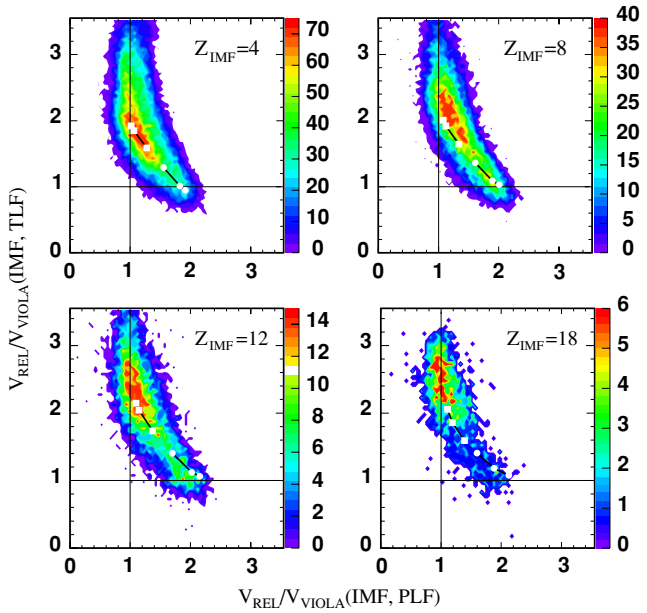

FIG. 7. (Color online) Correlation between relative velocities $V_{\rm rel}/V_{\rm Viola}$(IMF,PLF) and $V_{\rm rel}/V_{\rm Viola}$(IMF,TLF) for different intermediate mass fragments of $Z_{\rm IMF} = 4$, 8, 12, and 18. Color scale on the right-hand side of each panel shows the number of events per two-dimensional bin. The experimental distributions are compared with simple model calculations assuming that the IMF is released as a result of a two-step neck rupture process taking place 40, 80, or 120 fm/c after reseparation of the primary binary system. The shortest separation times (nearly prompt IMF emission) correspond to the location near the diagonal $V_{\rm rel}/V_{\rm Viola}$(IMF,PLF) = $V_{\rm rel}/V_{\rm Viola}$(IMF,TLF). Two branches of the calculated correlation correspond to either projectile breakup (upper branch) or target breakup (lower branch). For details of the calculation see the appendix.

C. Relative velocity correlations

Important information on the mechanism of ternary reactions can be obtained from analysis of relative velocities characterizing binary subsystems of the total three-body system. Specifically, we propose to analyze correlations between relative velocities of IMFs with respect to PLFs and TLFs, $V_{\rm rel}$(IMF,PLF) and $V_{\rm rel}$(IMF,TLF), respectively. In Fig. 7 we display two-dimensional plots of these relative velocities for four selected IMFs ($Z_{\rm IMF} = 4$, 8, 12, and 18). The relative velocities $V_{\rm rel}$(IMF,PLF) and $V_{\rm rel}$(IMF,TLF) are divided by the velocity $V_{\rm Viola}$ (see the appendix), corresponding to the kinetic energy of Coulomb repulsion for these systems as given by the Viola systematics [20] for the asymmetric split of a given system [21]. It can be readily checked that the correlation between the two relative velocities gives information on the scenario of the IMF formation, and particularly on the time when the IMF separates from PLF or TLF (or from both in the case of the instantaneous ternary split). In Fig. 7 we show loci of points representing $V_{\rm rel}/V_{\rm Viola}$(IMF,PLF) vs. $V_{\rm rel}/V_{\rm Viola}$(IMF,TLF) correlation, calculated assuming that the IMF separates either from the projectile (squares) or from target nucleus (circles) after a time interval of 40, 80,

or 120 fm/c elapsed from the primary (binary) separation of the projectile from the target at $t = 0$. (Details of this calculation are given in the appendix.) Events close to the diagonal in the $V_{\rm rel}/V_{\rm Viola}$(IMF,PLF) vs. $V_{\rm rel}/V_{\rm Viola}$(IMF,TLF) plots in Fig. 7 correspond to prompt ternary divisions, whereas those approaching $V_{\rm rel}/V_{\rm Viola}$(IMF,PLF) = 1 and $V_{\rm rel}/V_{\rm Viola}$(IMF,TLF) = 1 values correspond to the sequential split of the primary projectilelike nucleus or the targetlike nucleus, respectively. The time scale for all intermediate situations is rather short. It spans the time interval up to about 120–150 fm/c. Beyond that value, the predicted points of the $V_{\rm rel}/V_{\rm Viola}$(IMF,PLF) vs. $V_{\rm rel}/V_{\rm Viola}$(IMF,TLF) correlation move not further and are undistinguishable from much later "true" sequential decay processes. However, localization of the events clearly demonstrates that at least in case of *light* (most probable) IMFs, of $Z_{\rm IMF} \leqslant 8$, the majority of them are emitted in almost prompt or "fast two-step" processes, within times of about 40–80 fm/c.

Examining the correlation plots in Fig. 7, one can observe that generally there are more IMFs originating from the projectile breakup (upper branches) than from target breakup (lower branches). To some extent, this effect probably originates from the asymmetry of the colliding system but also is caused by the reduced efficiency for detection of TLFs within the limited angular range of the detecting system, $\theta \leqslant 30^\circ$.

It can be seen from the location of maxima of the relative velocity distributions in relation to the "time calibration" points in Fig. 7 that heavy IMFs ($Z_{\rm IMF} = 12$ and 18) are preferentially emitted not immediately after reseparation of the colliding nuclei, as is the case for $Z_{\rm IMF} = 4$, but rather in somewhat later stage, say at times of about 120 fm/c after the reseparation or even later. Such a process is thus intermediate between a genuine prompt ternary decay of the colliding system and true sequential decay of the projectile nucleus.

Within the time interval of about 100 fm/c the studied system moves over a distance of about 20 fm—comparable with its size. Therefore emission of heavy IMFs (e.g., Ar fragments; see Fig. 7, lower right panel) at times of about 120 fm/c after the beginning of reseparation, can still be associated with fragmentation of the neck formed between the nuclei after the collision. A two-step process, the double break of a massive neck stretched between the receding nuclei, in which the neck first separates from TLF, and then breaks away from PLF is a reasonable scenario explaining the deduced time intervals extending up to 120 fm/c and beyond. Conversely, events located near the diagonal in diagrams in Fig. 7 represent nearly prompt emission of predominantly light IMFs from the neck in its early stage of expansion, that is, when PLF and TLF still are in close contact.

One can speculate that to form heavy IMFs, such as Ar fragments, more matter is required in the neck region, that is, the neck must be considerably stretched and consequently the second break of the neck must happen after a longer time. This tendency is clearly seen in Fig. 7: with increasing $Z_{\rm IMF}$ the maximum of the distribution shifts toward longer IMF emission times.

The scenario of the IMF production presented above is consistent with simulations of semiperipheral nucleus-nucleus collisions in terms of the BNV stochastic transport model of Baran, Colonna, and Di Toro [10]. In this theoretical model, IMFs are also formed in the neck region and emitted approximately collinearly with the PLF-TLF axis, either promptly or "sequentially," as a result of the neck fragmentation mechanism. As an example, we show in Fig. 8 time distributions of the probability of formation of the neck remnants (IMFs or NOFs in the nomenclature of Ref. [10]), predicted with the model for different impact parameters in the range from 5 to 8 fm. Similarly as in Fig. 6, the presented distributions combine results for all IMFs, not differentiated according to their mass or charge and thus reflect in fact predictions for light IMFs. Comparison of these predictions with our "empirical" estimates of the emission time scale for light IMFs (upper panels in Fig. 7) shows very good agreement.

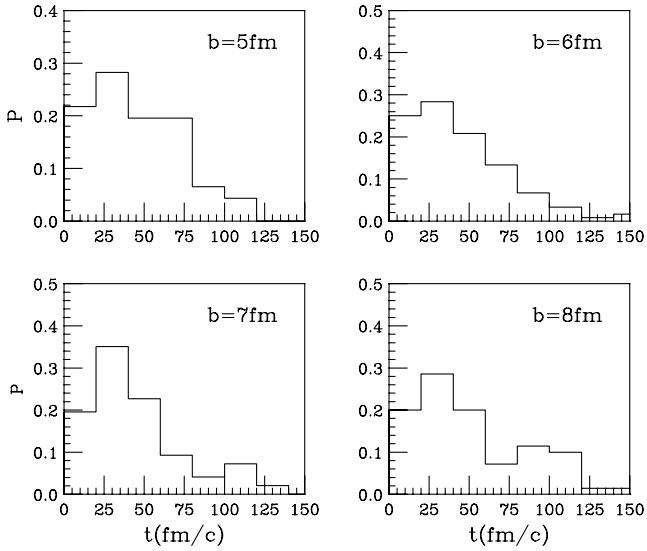

FIG. 8. Time distributions of the probability of formation of the neck remnants (IMFs) predicted with the stochastic BNV transport model [10] for different impact parameters.

It has been pointed out in Ref. [10] that after separation of the projectile nucleus from the target, large quadrupole and octupole deformations develop in both nuclei. Unfortunately prediction of further evolution of the deformation that might lead to emission of heavy IMFs is not possible in the present version of the BNV model. Consequently, production of heavy IMFs in a later stage of the reaction is considerably underpredicted.

IV. SUMMARY

We have analyzed semiperipheral collisions in the ^{124}Sn+^{64}Ni reaction at 35 MeV/nucleon by selecting nearly completely determined ternary events, in which the sum of atomic numbers of the three heaviest fragments was larger than 60. For so selected set of events a very useful and effective procedure of distinguishing PLFs from TLFs and IMFs, based on the correlation between charge of a fragment and its longitudinal velocity, was applied.

The observed ternary reactions involve emission of IMFs in a wide range of atomic numbers, up to $Z_{\rm IMF}$ of about 25. In all these reactions the IMFs are emitted preferentially with velocities intermediate between those of the PLF and TLF. This general feature is consistent with the scenario of IMF emission from the neck formed between projectile and target nuclei during the reseparation stage of the reaction.

A new method of data analysis has been proposed, which can be used for determination of the time scale of the IMF emission. Namely, the correlation between relative velocities in the IMF+PLF and IMF+TLF subsystems has been studied in the event-by-event regime for a selected class of events, in which the reaction is basically ternary involving three main fragments: PLF, TLF, and IMF. Localization of a given event in two-dimensional relative-velocity plot, $V_{\rm rel}/V_{\rm Viola}$(IMF, PLF) vs. $V_{\rm rel}/V_{\rm Viola}$(IMF,TLF), depends on the time t when the IMF is separated from PLF or TLF either in a two-step process (i.e., sequentially when $t > 0$) or almost instantly ($t \approx 0$), when all three fragments are still in close contact. Simple kinematical simulations can be used to "calibrate" the time scale in the $V_{\rm rel}/V_{\rm Viola}$(IMF,PLF) vs. $V_{\rm rel}/V_{\rm Viola}$(IMF,TLF) plots. We have shown that the majority of light IMFs are produced within 40–80 fm/c after the system starts to reseparate. On the average, lighter IMFs are produced earlier than heavier fragments. We found that heavy fragments of $Z_{\rm IMF} = 12$–18 are formed at times of about 120 fm/c after the reseparation, or later. Their emission can be viewed as resulting from two-step (sequential) neck rupture processes.

ACKNOWLEDGMENTS

We are grateful to R. Bassini, C. Boiano, C. Calí, V. Campagna, R. Cavaletti, O. Conti, M. D'Andrea, A. Di Stefano, F. Fichera, N. Giudice, A. Grimaldi, N. Guardone, H. Hong, P. Litrico, S. Marino, D. Moisa, D. Nicotra, G. Peirong, C. Rapicavoli, G. Rizza, S. Salomone, G. Saccá, V. Simion, and S. Urso for their invaluable help in assembling the forward part of CHIMERA. Thanks are due to C. Marchetta and E. Costa for preparing high-quality targets and also to D. Rifuggiato and L. Calabretta and their coworkers for delivering beams of perfect time characteristics. This work was supported in part by the Italian Ministero dell'Istruzione, dell'Università e della Ricerca (MIUR) under contract COFIN2002 and by NATO Grant PST.CLG.079417.

APPENDIX: THE TIME SCALE OF IMF EMISSION

The time scale of the IMF emission is estimated in a very simple one-dimensional calculation. It is assumed that in a semiperipheral collision of a projectile P and a target T, the binary (at first) system $P' + T'$ starts to reseparate along the beam direction having at the reseparation time $t = 0$ the relative velocity

$$V_{\rm rel}(P', T') = \alpha\, V_{\rm rel}(P, T), \tag{A1}$$

that is, the velocity reduced by a factor α with respect to the relative velocity of the system just before the collision. (The factor α can change from 0, for completely damped central collisions, to 1, for peripheral collisions without dissipation.)

A two-step-decay scenario is assumed: The IMF is emitted either from the projectile primary fragment P' at the time $t_{\rm sep}(P')$,

$$P + T \rightarrow P' + T', \qquad P' \rightarrow {\rm IMF} + {\rm PLF}, \tag{A2}$$

or from the target primary fragment T' at the time $t_{\rm sep}(T')$:

$$P + T \rightarrow P' + T', \qquad T' \rightarrow {\rm IMF} + {\rm TLF}. \tag{A3}$$

From the reseparation at $t = 0$ to the time of releasing the IMF, the fragments P' and T' move in their mutual Coulomb repulsion field. We have to emphasize, however, that the idealized two-step scenario of Eqs. (A2) and (A3) is only a rough approximation of a much more complex, dynamic process in which a "neck" is probably formed between P' and T' and the IMF is likely to be a *remnant of the neck*, created as a result of the double *sequential* rupture of this neck.

The mass and charge of of P' and T' may be influenced by the exchange of mass and charge between P and T, as well as by the process of the neck formation suggested above. Therefore, masses and charges of the final fragments PLF, TLF, and IMF in the postulated processes (A2) and (A3) are not predefined. In our simplified calculation, we assume that the IMF is formed from the matter of both, projectile and target, proportionally to their initial masses and charges. (This assumption is consistent with the idea of IMFs being remnants of the neck.) Therefore for a given intermediate mass fragment of $Z_{\rm IMF}$ and $A_{\rm IMF}$, the charge and mass numbers of the respective PLF are fixed as follows:

$$Z_{\rm PLF} = Z_P - Z_{\rm IMF}\frac{Z_P}{Z_P + Z_T}, \tag{A4}$$

$$A_{\rm PLF} = A_P - A_{\rm IMF}\frac{A_P}{A_P + A_T}, \tag{A5}$$

and analog expressions hold for $Z_{\rm TLF}$ and $A_{\rm TLF}$.

To reproduce the observed final velocities of PLF, TLF, and IMF, it was necessary to assume that nuclear matter that is used to form the IMF (presumably the matter in the neck) has *continuous* velocity distribution. In case of the breakup of P', Eq. (A2), the starting velocity of the IMF is assumed to change from $V'_{\rm mid} = \frac{1}{2}(V_{P'} + V_{T'})$ to $V_{P'}$, proportionally to the surface-to-surface distance $D_{\rm sep} = r - R(P') - R(T')$ between P' and T', at which the separation of IMF (from PLF) takes place at the time $t_{\rm sep}(P')$:

$$V_{\rm IMF}[t_{\rm sep}(P')] = V'_{\rm mid} + (V_{P'} - V'_{\rm mid})\frac{D_{\rm sep}}{D_0}. \tag{A6}$$

Similarly in case of the breakup of T', Eq. (A3), at the time $t_{\rm sep}(T')$,

$$V_{\rm IMF}[t_{\rm sep}(T')] = V'_{\rm mid} + (V_{T'} - V'_{\rm mid})\frac{D_{\rm sep}}{D_0}. \tag{A7}$$

Here D_0 is the surface-to-surface distance $D_{\rm sep}$, at which both velocities, $V_{\rm IMF}$ and $V_{\rm PLF}$ (or $V_{\rm IMF}$ and $V_{\rm TLF}$), eventually become equal. [For $D_{\rm sep} > D_0$, $V_{\rm IMF}(t_{\rm sep}) = V_{P'}$ in case of the P' breakup, and $V_{\rm IMF}(t_{\rm sep}) = V_{T'}$ in case of the T' breakup.]

We assumed in the calculation that $D_0 = R(P') + R(T')$, a typical length of the neck in fission reactions.

Following the separation time $t_{sep}(P')$ or $t_{sep}(T')$, all three fragments, PLF, TLF, and IMF, move in the field of mutual Coulomb interaction. For simplicity, it is assumed that the IMF is released collinearly with the velocity vectors of PLF and TLF, and thus the final velocities of PLF, TLF, and IMF are integrated numerically only in one dimension.

Our method of analysis gives a possibility to determine the separation time t_{sep} from the correlation between relative velocities V_{rel}(IMF,PLF) and V_{rel}(IMF,TLF). Individual velocities V_{IMF}, V_{PLF}, and V_{TLF} are taken in infinity, and their differences $V_{rel}(\text{IMF, PLF}) = V_{PLF} - V_{IMF}$ and $V_{rel}(\text{IMF, TLF}) = V_{IMF} - V_{TLF}$ are expressed in units corresponding to the kinetic energy of Coulomb repulsion, given by the Viola systematics [20] modified for asymmetric split [21] as follows:

$$V_{\text{Viola}} = \sqrt{\frac{2}{\mu}\left(\frac{0.755\, Z_1 Z_2}{A_1^{1/3} + A_2^{1/3}} + 7.3\,\text{MeV}\right)}, \qquad \text{(A8)}$$

where μ is the reduced mass of the decaying subsystem.

The predicted correlation between V_{rel}/V_{Viola}(IMF, PLF) and V_{rel}/V_{Viola}(IMF,TLF) is shown in Fig. 7 for assumed separation times $t_{sep}(P')$ (squares) and $t_{sep}(T')$ (circles) equal to 40, 80, and 120 fm/c. The loci of the predicted points coincide with experimental distributions when *all three* relative velocities, including V_{rel}(PLF,TLF), are correctly predicted. To obtain the latter in agreement with the observed average velocities $\langle V_{PLF}\rangle$ and $\langle V_{TLF}\rangle$ (see Fig. 3), it was necessary to assume approximately 20% reduction of the relative velocity in the first stage of the collision, $\alpha = 0.8$ in Eq. (A1).

[1] W. U. Schröder and J. Tōke, in *Nonequilibrium Physics at Short Time Scales*, edited by K. Morawetz (Springer-Verlag, Berlin/Heidelberg/New York, 2004), p. 417.
[2] C. P. Montoya *et al.*, Phys. Rev. Lett. **73**, 3070 (1994).
[3] J. F. Lecolley *et al.*, Phys. Lett. **B354**, 202 (1995).
[4] J. Tōke *et al.*, Nucl. Phys. **A583**, 519 (1995).
[5] A. A. Stefanini *et al.*, Z. Phys. A **351**, 167 (1995).
[6] E. Plagnol *et al.*, Phys. Rev. C **61**, 014606 (1999).
[7] P. Milazzo *et al.*, Phys. Lett. **B509**, 204 (2001).
[8] B. Borderie, J. Phys. G Nucl. Part. Phys. **28**, 217(R) (2002).
[9] P. Chomaz, M. Colonna, and J. Randrup, Phys. Rep. **389**, 263 (2004).
[10] V. Baran, M. Colonna, and M. Di Toro, Nucl. Phys. **A730**, 329 (2004).
[11] F. Bocage *et al.*, Nucl. Phys. **A676**, 391 (2000).
[12] J. Colin *et al.*, Phys. Rev. C **67**, 064603 (2003).
[13] E. De Filippo *et al.*, submitted to Phys. Rev. C.
[14] A. Pagano *et al.*, Nucl. Phys. **A681**, 331 (2001).
[15] A. Pagano *et al.*, Nucl. Phys. **A734**, 504 (2004).
[16] S. Aiello *et al.*, Nucl. Phys. **A583**, 461 (1995); Nucl. Instrum. Methods A **369**, 50 (1996); **400**, 469 (1997).
[17] A. Alderighi *et al.*, Nucl. Instrum. Methods A **489**, 257 (2002).
[18] N. Le Neindre *et al.*, Nucl. Instrum. Methods A **490**, 251 (2002).
[19] E. Geraci *et al.*, Nucl. Phys. **A732**, 173 (2004).
[20] V. E. Viola, K. Kwiatkowski, and M. Walker, Phys. Rev. C **31**, 1550 (1985).
[21] D. J. Hinde, J. R. Leigh, J. J. M. Bokhorst, J. O. Newton, R. L. Walsh, and J. E. Boldeman, Nucl. Phys. **A472**, 318 (1987).